Pergamon

0021-8502(95)00542-0

J. Aerosol Sci., Vol. 27, No. 2, pp. 263–280, 1996

0021-8502/96 $15.00 + 0.00

AN ANALYTICAL MODEL FOR AEROSOL FILTRATION BY NONUNIFORM FILTER MEDIA*

Michael Shapiro

Faculty of Mechanical Engineering, Technion—Israel Institute of Technology, Haifa 32000, Israel

(*First received* 10 *October* 1994; *and in revised form* 25 *August* 1995)

Abstract—Filtration of submicrometer aerosol particles by nonhomogeneous porous filters is studied analytically. The effect of inhomogeneities is to cause nonuniform pressure gradient and concomitant curvilinear mesoscale air streamlines within the filtering material. A general equation governing change of aerosol filtration length along curved air streamlines is developed.

Analytical analyses are performed for a homogeneous bulk filter material containing a small volumetric fraction, α, of spatial inhomogeneities (inclusions). An expression is derived for the effective filtration length of such a composite filter material, relative to the comparable length of the corresponding uniform matrix and the filtering properties of the inclusions.

Calculations performed for spherical inclusions show that they tend to decrease the aerosol filtration efficiency when their porosity is less than that of the surrounding filter medium. However, the effect of inclusions with porosity exceeding that of the filter material is to decrease the aerosol filtration length, i.e. to enhance the aerosol collection rate.

The model was tested by experiments performed for submicrometer aerosols, collected in a granular bed filter. It was composed of 1.4 mm spherical glass beads, forming a homogeneous matrix, and 15 mm balls, serving as impermeable inclusions. For such a medium the model predicts a nonmonotonic α-dependence of the effective filtration length, which qualitatively agrees with the experimental data.

1. INTRODUCTION

Classical filtration theory (Dorman, 1974; Pich, 1966; Davies, 1973) treats the filtration problem by calculating the aerosol collection rate on a single filter element, the size and shape of which are chosen to best represent the microstructure and porosity of a given filtering material. The filtration efficiency η is calculated by summing up the contributions of all such elements to yield

$$\eta = 1 - \frac{\bar{n}_{\text{out}}}{\bar{n}_{\text{in}}} = 1 - \exp(-L/l), \tag{1}$$

where $\bar{n}_{\text{in}}$, $\bar{n}_{\text{out}}$ are the respective aerosol concentrations in the inlet and the outlet of a filter of thickness L, and l is the characteristic filtration length (Leers, 1957). Known models for the evaluation of l include those based on single element efficiency (Davis, 1973; Brown, 1993) and dispersion–reaction theory of aerosol filtration (Shapiro and Brenner, 1990; Shapiro *et al.*, 1991).

The above approaches assume that the filter medium is *macroscopically* homogeneous. One example of such filters is packed beds of granules (Tardos *et al.*, 1978) of similar shapes and sizes (e.g. sand beds). However, fibrous filters are oftentimes characterized by nonuniformities of different sizes, distributed within the filter medium. These nonuniformities are known to produce a strong effect on the filtration properties. In some cases they lead to an increase of penetration of submicrometer aerosols by a several-fold factor (Lücke *et al.*, 1993).

The existence of structural nonuniformities introduces an additional length-scale into the hierarchy of scales existing in all porous materials (Adler, 1992). Normally these scales

*Presented at the 4th International Aerosol Conference, Los Angeles, 29 August–2 September 1994.

include microscale (of the order of the collector size, d), used for the description of interstitial aerosol transport and collection, and macroscale, comparable to the filter external size, L. In addition to the above, in nonuniform filter materials there exists an intermediate, or *mesoscale a*, characterizing the average size of nonuniformities, however, still much larger than collector diameter d, or the average interstitial pore size. Accordingly, at this mesoscale the filter is viewed as a continuum with spatially nonuniform properties.

The effect of spatial inhomogeneities is to produce a nonuniform mesoscale pressure gradient distribution within the filter material. Since this pressure gradient is proportional to the local mesoscale velocity via Darcy's law (Bear,1972), aerosol particles move in different parts of the filter material with different mesoscale velocities. This nonuniform mesoscale velocity distribution results in different *microscopic* velocity fields (prevailing around each collector element). Therefore, particle collection mechanisms may change along the mesoscale streamlines. As such, different parts of the filter material may collect aerosol particles at different rates.

The overall effect of the above processes on the filtration efficiency depends on the nonhomogeneous structure of the filter material (e.g. size, shape and porosity distributions of inhomogeneities) as well as on the spatial variations of the collector size and orientation distributions. If this information is known, for example, by means of a detailed investigation of each given nonhomogeneous filter, classical filtration concepts can be applied to calculation of the aerosol collection rate (Schweers and Löffler, 1993), with the above detailed information being accounted for in appropriate numerical calculational models. In general, one can state that the more we know about the nonuniform nature of the filter material, the better we can predict its filtration efficiency.

Measurements of the above meso- and microscale filter properties (Lücke *et al.*, 1993) and computer calculations accounting for this extensive information constitute very difficult tasks. It may turn out that several parameters, employed in such calculations, such as angular distribution of the collector elements, are unnecessary for the majority of filter materials. As such, an important problem deserving special attention is characterization of the nonhomogeneous filter structure by easily measurable parameters and their incorporation in simple and efficient models for calculating aerosol collection rates. Towards this goal, in this paper we attempt to devise a basic model of aerosol filtration by spatially nonhomogeneous filter materials, which is amenable to analytical analyses.

2. PHYSICAL MODEL

The filter material is assumed to be a uniform matrix, containing a certain volumetric fraction α of inclusions of size a (see Fig. 1). Both inside and outside the inclusions, the filter structure is assumed to be homogeneous, albeit with different porosities. The filter medium porosity ε is, thus, a piecewise continuous function:

$$\varepsilon = \begin{cases} \varepsilon_1 & \text{outside inclusions,} \\ \varepsilon_2 & \text{inside inclusions,} \end{cases} \tag{2}$$

where, generally, $\varepsilon_1 \neq \varepsilon_2$. The total filter void fraction may be expressed as

$$\bar{\varepsilon} = \alpha\varepsilon_2 + (1 - \alpha)\varepsilon_1 . \tag{3}$$

We assume the size a of the inclusions to be much smaller than the characteristic filter dimension L, but much larger than the mean distance between the collector elements, y_i, either inside, or outside the inclusions. The distance y_i is related to the collector diameter d via the porosity as

$$d^n/y_i^n = 1 - \varepsilon_i, \quad i = 1, 2,$$

where $n = 2$ for cylindrical and $n = 3$ for spherical collectors. This yields

$$y_i = d(1 - \varepsilon_i)^{-1/n},$$

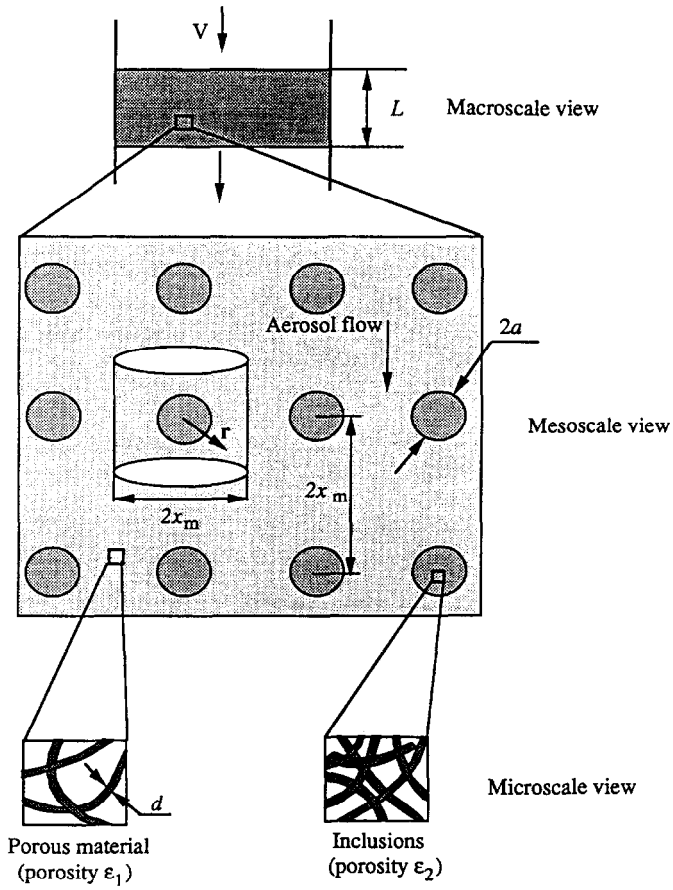

Fig. 1. Schematic of the mesoscale filter geometry and aerosol flow between the successive layers of inclusions.

and the constraints imposed upon a are

$$d(1-\varepsilon_i)^{-1/n} \ll a \ll L, \quad i = 1, 2. \tag{4}$$

In particular, for $i = 2$ the above left inequality means that each of the inclusions contains sufficiently many collector elements. Inequality (4) defines an intermediate (meso-) length-scale a, which characterizes the filter nonhomogeneous structure.

The above simplistic model is not aimed at describing in a detailed manner non-homogeneous structures of industrial filters. In granular bed filters, inhomogeneities may be associated with local variations of the granular sizes, especially when beds are composed of polydisperse granules which are not well mixed. Sometimes combinations of granules are used, the sizes of which differ significantly (Ives, 1989). Large granules (of size a) form inclusions and smaller granules (of size d) filling the voids between the large ones serve as a porous matrix. In this case $\varepsilon_2 = 0$, and the model proposed here may be used to rationalize the choice of the granular sizes (a and d) and the volumetric fraction α of the above bidisperse granular distribution.

In fibrous filters, inhomogeneities are usually formed by irregular structures embedded within flat fibrous sheets. The size a of these structures may not be small to comply with inequality (4) and, hence, may not correspond to an idealized geometric model here considered. In fact, the model (2)–(4) is but a particular case of a more general situation, where one can specify arbitrary meso- or even macrostructural inhomogeneities, as embodied in the distributions of porosity, ε, permeability, κ, fiber diameter, and orientation:

$$\varepsilon = \varepsilon(\mathbf{r}), \quad \kappa = \kappa(\mathbf{r}), \text{ etc.}$$

Such an approach was attempted by Schweers and Löffler (1993) and Lajos (1985), who subdivided the filter in a lattice of volume elements of size $a < L$, each characterized by its own structure. This can be described by considering porosity, permeability, etc., as piecewise continuous functions of a mesoscale spatial position $\mathbf{r}$. A particular case, where such spatial elements differ only by their porosity (and permeability), with all other properties being identical, clearly falls within the scope of model (2).

The present treatment is aimed at calculation of the macroscopic properties (at the length-scale L) of the filter medium, i.e. its characteristic pressure drop and the overall aerosol characteristic filtration length, provided that these quantities are known at the mesoscale. We, thus, calculate the aerosol filtration rate in a representative mesoscale filter volume element, surrounding one inclusion (see Fig. 1). The first step towards this goal is calculation of the mesoscale air velocity distribution in this element.

3. MESOSCALE VELOCITY DISTRIBUTION WITHIN A NONUNIFORM FILTER MATERIAL

Denote the permeabilities of the filter matrix and of the inclusions by κ_1 and κ_2, respectively. That is, the permeability $\kappa(\mathbf{r})$ of the composite filter material is

$$\kappa = \begin{cases} \kappa_1 & \text{outside } \tau, \\ \kappa_2 & \text{inside } \tau, \end{cases} \tag{5}$$

where τ is the volume domain inside each inclusion and $\mathbf{r}$ is the mesoscale position vector. We assume that Darcy's law (Bear, 1972) is valid everywhere, i.e.

$$\nabla \cdot \mathbf{V} = 0, \quad \mathbf{V} = -\frac{\kappa}{\mu} \nabla P, \tag{6a, b}$$

where $\nabla = \partial/\partial \mathbf{r}$; $\mathbf{V}(\mathbf{r})$, $P(\mathbf{r})$ are the mesoscale air velocity and pressure fields and μ is the air dynamic viscosity.*

The pressure distribution within the filter material is obtained by eliminating the velocity from equations (6a, b), which yields Laplace's equation

$$\nabla^2 P = 0 \quad \text{inside and outside } \tau. \tag{7}$$

This is to be solved subject to the following boundary conditions:

$$P - \text{continuous across } \partial\tau, \tag{8a}$$

$$\kappa_1 \boldsymbol{\nu} \cdot \nabla P = \kappa_2 \boldsymbol{\nu} \cdot \nabla P, \quad \mathbf{r} \in \partial\tau, \tag{8b}$$

expressing continuity of the pressure and the velocity component normal to the interface $\partial\tau$ separating two porous materials with $\boldsymbol{\nu}$ being the unit vector normal to $\partial\tau$ (see Fig. 2). For a small volumetric fraction α, equations (7) and (8) are solved for a single inclusion subject to the condition to uniformity of the air flow velocity at a large distance from τ. This may be expressed in terms of the cylindrical coordinates r, z, θ (see Fig. 2) in the form

$$P = \left(\frac{\mathrm{d}P}{\mathrm{d}z}\right)_\infty r\cos\theta + \text{const} = -\frac{\mu}{\kappa_1} V_\infty r\cos\theta + \text{const} \quad \text{as } r \to \infty. \tag{9}$$

In the above the constants $(\mathrm{d}P/\mathrm{d}z)_\infty$ and

$$V_\infty = -\kappa_1 (\mathrm{d}P/\mathrm{d}z)_\infty / \mu \tag{10}$$

are the pressure gradient and the air velocity far from the inclusion respectively.

In the situation where α is not small, equation (9) cannot be used. In this case equations (7) and (8) are solved in the whole filter material subject to the condition $\kappa_1 \boldsymbol{\nu} \cdot \nabla P = 0$,

*One should note that the above velocity and pressure fields are different from their microscale counterparts $\mathbf{v}$, p, defined at the *interstitial*, or microscale.

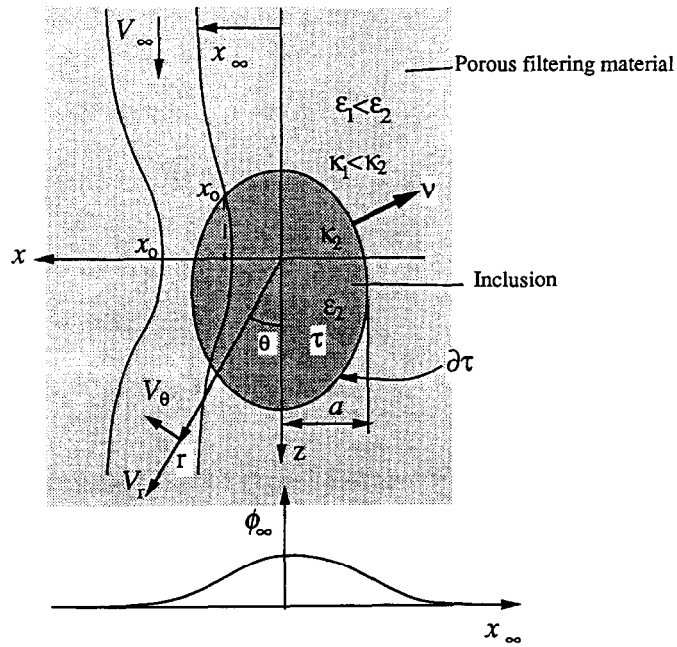

Fig. 2. Aerosol mesoscale streamlines near an inclusion placed within a homogeneous filtering material.

imposed on the filter walls. Mathematically this represents a particular case of equation (8b), where $\kappa_2 = 0$. Equation (7) may be solved for any porosity distribution within the filter by the application of known methods of mathematical physics. The solution for this problem may be used to calculate the mesoscale air flow trajectories, required for calculation of the aerosol deposition [see equations (19)–(23)].

Below we derive an approximate solution (7)–(9) in a particulate case, where $\alpha \ll 1$. Specifically we are interested in a solution at large distances from a single inclusion. This will prove useful in deriving a general functional form for the effective filtration length (see Section 4).

Assuming, for simplicity, axisymmetric inclusions, the large r solution may be shown to possess the following general from (Morse and Feshbach, 1953):

$$P(r,\theta) \approx \left(\frac{dP}{dz}\right)_\infty \left[\sum_{k=0}^{\infty} A_k P_k(\cos\theta)\left(\frac{a}{r}\right)^{k+2} + \cos\theta\right] r + \text{const} \quad r \to \infty, \tag{11}$$

where $P_k(x)$ is the kth Legendre polynomial and A_k ($k = 0, 1, \ldots$) are constant coefficients. One can further use equations (6a, b) to show that

$$\int_{S_0} \nabla P \cdot d\mathbf{S} = 0, \tag{12}$$

where dS is the surface element on any surface S_0 surrounding the inclusion. Substituting P given by equation (11) into equation (12) and choosing S_0 as a sphere of a sufficiently large radius $r = r_0$, one obtains that all terms in the infinite series in equation (11) vanish except $k = 0$, for which $P_0(\cos\theta) = 1$. This immediately yields $A_0 = 0$. Therefore, for large r the solution for the pressure field is

$$P(r,\theta) \approx \left(\frac{dP}{dz}\right)_\infty \left[A_1\left(\frac{a}{r}\right)^3 + 1\right] r\cos\theta + O(r^{-3}), \quad r \to \infty. \tag{13}$$

The components of the velocity field far from the inclusion are obtained by the introduction of equation (13) into equation (6b):

$$V_r = V_\infty(1 - 2A_1 a^3/r^3)\cos\theta + O(r^{-4}), \quad r \gg a, \tag{14a}$$

$$V_\theta = -V_\infty(1 + A_1 a^3/r^3)\sin\theta + O(r^{-4}), \quad r \gg a. \tag{14b}$$

The air flow streamlines through the porous filter material are obtained from the differential equation

$$\frac{1}{r}\frac{dr}{d\theta} = \frac{V_r}{V_\theta}. \tag{15}$$

Upon substitution of equation (15) into equations (14a, b) and integration, one obtains

$$r\sin\theta\sqrt{1-\frac{2A_1a^3}{r^3}+O(r^{-3})} = x_\infty, \quad r \gg a, \tag{16}$$

where x_∞ is an integration constant, representing the distance between the streamline and the z-axis at $r \to \infty$ (see Fig. 2). This equation shows that far from the inclusion the streamlines tend to straight lines $x_\infty = \text{const}$ parallel to the z-axis. The x- and z-velocity components may be obtained from equations (14a, b) by means of the relationships $V_z = V_r\cos\theta - V_\theta\sin\theta$, $V_x = V_r\sin\theta + V_\theta\cos\theta$.

In Section 5 we use the large r solution form (13) and (16) for a general estimate of the effective filtration length of the nonhomogeneous filter material.

4. AEROSOL TRANSPORT AND DEPOSITION WITHIN UNIFORM FILTER MATERIALS

As one can see from equations (14a, b), the mesoscale flow velocity field in the region exterior to the inclusion is nonuniform and gradually approaches the uniform flow for $r \to \infty$. In the latter undisturbed region the following mesoscale aerosol transport and deposition equation is valid (Shapiro and Brenner, 1990; Shapiro *et al.*, 1991):

$$U_{z_\infty}\frac{dn_\infty}{dz} - D_{z_\infty}\frac{d^2n_\infty}{dz^2} + K_{z_\infty}n_\infty = 0, \tag{17}$$

where $n_\infty = n_\infty(z)$ is the mesoscale aerosol concentration far from the inclusion, and the *constant* coefficients $U_{z_\infty}, D_{z_\infty}, K_{z_\infty}$ are the mesoscale aerosol velocity, diffusivity and volumetric deposition coefficient in the uniform filter matrix.† These quantities may be calculated from the microscale unit cell analysis, as outlined in the dispersion–reaction theory of aerosol filtration. In particular, it has been shown that in many practically important situations encountered in aerosol filtration the diffusive term in equation (17) may be neglected. Therefore, equation (17) may be rewritten in the form

$$\frac{dn_\infty}{dz} + \frac{1}{l_\infty}n_\infty = 0, \tag{18a}$$

where

$$l_\infty = U_{z_\infty}/K_{z_\infty} \tag{18b}$$

is the characteristic filtration length of the material, prevailing far from the inclusion.

Equation (18a) is generalized to include spatial dependence of the mesoscale aerosol transport coefficients

$$\nabla\cdot[\mathbf{U}(\mathbf{r})n - \mathbf{D}(\mathbf{r})\cdot\nabla n] + K(\mathbf{r})n = 0, \tag{19}$$

where $n(\mathbf{r})$ is the aerosol mesoscale concentration and $\mathbf{U}(\mathbf{r})$, $\mathbf{D}(\mathbf{r})$, $K(\mathbf{r})$ are the mesoscale *position-dependent* transport coefficients. These may be calculated from the dispersion–reaction aerosol filtration model by assuming it to be applicable locally at *every point* $\mathbf{r}$, using the local value $\mathbf{V}(\mathbf{r})$ of the air velocity. This assumption of the local applicability of

†Note that, generally, aerosol velocity U_{z_∞} differs from air velocity V_∞ (Shapiro *et al.*, 1991).

the dispersion–reaction model and the mesoscale equation (19) is similar to the assumption of the local thermodynamic equilibrium, used in the heat transfer theory (Bird *et al.*, 1960), which enables one to consider the heat transport equation with variable (position-dependent) transport coefficients.

A general condition of applicability of equation (19) is that the characteristic distance, on which the air velocity changes appreciably, is much larger than the interstitial scales $d(1-\varepsilon_i)^{-1/n}$. This characteristic distance is of order a [e.g. see equations (14a, b)]. Therefore, the condition of validity of equation (19) is

$$a \gg d(1-\varepsilon_i)^{-1/3}, \quad i = 1, 2,$$

which accords with the left inequality of equation (4). In fact, the above inequality also provides the condition of applicability of the Darcy's equations (6a, b) (Adler, 1992).

In accordance with the assumption made in the derivation of equation (18a), we further omit the aerosol mesoscale diffusion (dispersion) term in equation (19) as negligible. With this simplification one can show that in the absence of external forces $\mathbf{U}$ is proportional to $\mathbf{V}$ (Shapiro *et al.*, 1991) and, hence, $\nabla\cdot\mathbf{U} \propto \nabla\cdot\mathbf{V} = 0$ [see equation (6a)]. This allows to rewrite equation (19) in the form

$$\mathbf{U}(\mathbf{r})\cdot\nabla n + K(\mathbf{r})n = 0. \tag{20}$$

In order to solve this equation for $n(\mathbf{r})$, one should calculate $\mathbf{U}(\mathbf{r})$ and $K(\mathbf{r})$ at every point $\mathbf{r}$ employing the dispersion–reaction theory and using the local value of $\mathbf{V}(\mathbf{r})$ calculated from problem (7)–(9). Rather than follow this straightforward but computationally difficult route, we use the fact that $\mathbf{U}(\mathbf{r})$ is parallel to $\mathbf{V}(\mathbf{r})$. This allows to rewrite equation (20) in the following form:

$$\frac{\mathrm{d}n}{\mathrm{d}s} + \frac{1}{l(s)}n = 0, \tag{21}$$

wherein $l(s) = U(s)/K(s)$ is the local filtration length and the coordinate s is measured along the streamlines, which now may also be viewed as aerosol mesoscale trajectories.

Equation (21) implies that aerosol particles move only along the air streamlines, without either longitudinal or lateral diffusion at the mesoscale. This assumption is valid at short distances (of order a), as measured by the characteristic Peclet number (Shapiro and Brenner, 1990). However, the role of aerosol diffusion is very important on a larger scale, where its effect is to remix aerosol particles far downstream after each layer of inclusions (see Section 5 for a discussion on this matter).

In order to integrate equation (21), one should specify how the characteristic filtration length changes along the aerosol trajectories. For submicrometer aerosols, whose deposition is governed by the Brownian diffusivity D, one can generically write

$$l \propto \psi(\varepsilon)\mathrm{Pe}^k, \tag{22}$$

where $\mathrm{Pe} = Vd/D$ is the characteristic microscale Péclet number based on the collector diameter, ψ is a porosity-dependent function (Davis, 1973) and k is a constant varying between 2/3 for random arrays (Levich, 1962; Tardos *et al.*, 1978) and 1 for ordered arrays (Shapiro *et al.*, 1991).

From equation (22) one can deduce that the local characteristic filtration length changes with s in accordance with the relations

$$l(s) = l_\infty \left[\frac{V(s)}{V_\infty}\right]^k \quad \text{outside the inclusion,} \tag{23a}$$

$$l(s) = l_\infty \frac{\psi(\varepsilon_2)}{\psi(\varepsilon_1)}\left[\frac{V(s)}{V_\infty}\right]^k \quad \text{inside the inclusion,} \tag{23b}$$

where l_∞ and V_∞ are given by equations (18b) and (10), respectively, and the absolute value of the air velocity, $V(s) = [V_r^2(s) + V_\theta^2(s)]^{1/2}$, is calculated from the solution of the problem (7)–(9).

We will use equations (22) and (23) with $k = 1$, although the results to be derived may be obtained with other values of k and also with additional deposition mechanisms which can be incorporated in equation (22).

Equation (21) with $l(s)$ given by equations (23a, b) may be solved to yield the mesoscale aerosol concentration field $n = n(s)$ everywhere in the nonuniform filter medium, i.e. both inside and outside the inclusions. It may be solved with *any* air velocity field $V(s)$, obtained from the solution of the Darcy's equations (6a, b) with an arbitrary specified permeability distribution $\kappa(\mathbf{r})$ [not necessarily the one given in equation (5)]. In the following we do this using asymptotic solution (13), (14), (16), obtained for small volumetric fraction α. It will eventually turn out that in this case one can approximately solve equation (21) and determine the functional form of the *effective* characteristic filtration length $\bar{l}$ of a nonuniform filtering material, which characterizes the efficiency of the aerosol filtration process at the macroscale.

5. EFFECTIVE FILTRATION LENGTH OF THE NONHOMOGENEOUS FILTER MEDIUM

Equation (21) may be integrated by separating variables

$$\ln n = -\int \frac{\mathrm{d}s}{l(s)}. \tag{24}$$

The local filtration length $l(s)$ may be expressed in the form (see also Fig. 2)

$$l(s) = l(z, x_\infty),$$

where the coordinate z is measured from the center of an axisymmetric inclusion. Moreover, one can see from the asymptotic solutions (14), (16) and (23a) that

$$l(z, x_\infty) = l_\infty [1 + f(z, x_\infty)], \tag{25a}$$

$$\mathrm{d}s = \mathrm{d}z\sqrt{1 + (V_x/V_z)^2} = \mathrm{d}z [1 + f_1(z, x_\infty)], \tag{25b}$$

where

$$f(z, x_\infty), f_1(z, x_\infty) = O(r^{-3}) \quad \text{as } r = (z^2 + x_\infty^2)^{1/2} \to \infty. \tag{26}$$

Using equations (25a, b) in equation (24) and performing integration with respect to the dimensionless variable[‡] $\tilde{z} = z/a$ from $\tilde{z} = -\infty$ to a current position $\tilde{z}$, one obtains

$$\ln n(\tilde{z}, \tilde{x}_\infty) = -a\frac{\tilde{z} + \phi(\tilde{z}, \tilde{x}_\infty)}{l_\infty} + \text{const}, \tag{27}$$

wherein also $\tilde{x}_\infty = x_\infty/a$, and

$$\phi(\tilde{z}, \tilde{x}_\infty) = -\int_{-\infty}^{\tilde{z}} \frac{f_1(\tilde{z}, \tilde{x}_\infty) - f(\tilde{z}, \tilde{x}_\infty)}{1 + f(\tilde{z}, \tilde{x}_\infty)} \mathrm{d}\tilde{z} \to 0 \quad \text{as } \tilde{z} \to -\infty. \tag{28}$$

In the absence of inclusions (uniform filter material) $l(\tilde{z}, \tilde{x}_\infty) = l_\infty = \text{const}$ everywhere and the solution for the aerosol concentration distribution is

$$\ln n_\infty(\tilde{z}) = -\frac{a}{l_\infty}\tilde{z} + \text{const}. \tag{29}$$

Eliminating the constant from equations (27) and (29), one obtains

$$n(\tilde{z}, \tilde{x}_\infty) = n_\infty(\tilde{z}) \exp\left(-\frac{a}{l_\infty}\phi(\tilde{z}, \tilde{x}_\infty)\right), \tag{30}$$

[‡]In this section we mark by a tilde all dimensionless distances normalized by the radius a of the inclusions. All variables with the overbar pertain to the macroscale.

wherein we have assumed that the concentration distribution far upstream before the inclusion is uniform, i.e. depends only on $\tilde{z}$ but not on $\tilde{x}_\infty$.

For any fixed $\tilde{x}_\infty$ the integrand function in equation (28) vanishes as $\tilde{z}^{-3}$ with increasing $\tilde{z}$ [see equation (26)]. Hence, for $\tilde{z} \to \infty$ the integral in equation (28) converges and yields

$$\phi(\tilde{z}, \tilde{x}_\infty) \to \phi_\infty(\tilde{x}_\infty) \equiv -\int_{-\infty}^{\infty} \frac{f_1(\tilde{z}, \tilde{x}_\infty) - f(\tilde{z}, \tilde{x}_\infty)}{1 + f(\tilde{z}, \tilde{x}_\infty)} d\tilde{z} \quad \text{as } \tilde{r} \to \infty. \tag{31a}$$

In view of relation (26) the integral value $\phi_\infty(\tilde{x}_\infty)$ exhibits the following large $\tilde{x}_\infty$ behavior:

$$\phi_\infty(\tilde{x}_\infty) = O(\tilde{x}_\infty^{-2}) = B_1 \tilde{x}_\infty^{-2} + o(\tilde{x}_\infty^{-2}) \quad \text{as } \tilde{x}_\infty \to \infty, \tag{31b}$$

with $B_1 = \text{const.}$

The function $\phi_\infty(\tilde{x}_\infty)$ describes the influence of inclusions on the downstream mesoscale aerosol concentration. This function is affected by the following two factors, both, however, stemming from the presence of inclusion:

(i) Increase of the total length of the aerosol pass (see Fig. 2). Far from the inclusion the effect of this factor is controlled by the coefficient A_1, appearing in equations (13), (14) and (16). Explicitly, with increasing $|A_1 - 1|$ the air flow trajectories become more curved, which leads to larger $\phi_\infty(\tilde{x}_\infty)$.

(ii) Deviation of the local filtration length from its limiting value at infinity [see equations (23a) and (25a)]. For less permeable inclusions ($\kappa_2 < \kappa_1$) this factor may be shown to increase $\phi_\infty(\tilde{x}_\infty)$ for those trajectories which pass exterior to the inclusions.

In all cases, however, the effects of both of the above factors vanish far from each inclusion in accordance with equation (31b).

We now calculate the aerosol concentration distribution far downstream from the inclusion. It is given by equation (30) upon replacing $\phi(\tilde{z}, \tilde{x}_\infty)$ by $\phi_\infty(\tilde{x}_\infty)$ there:

$$n(\tilde{z}, \tilde{x}_\infty) = n_\infty(\tilde{z}) \exp\left(-\frac{a}{l_\infty}\phi_\infty(\tilde{x}_\infty)\right). \tag{32}$$

One can see, therefore, that the downstream aerosol concentration is nonuniform (depends on the lateral coordinate $\tilde{x}_\infty$). This result is used to calculate the *area-averaged* concentration at the downstream location from a layer of inclusions separated by an average distance $2x_m$ (see Fig. 1). Towards this goal, integrate equation (32) over the circular area of radius x_m, to obtain

$$\bar{n}(\tilde{z}) = n_\infty(\tilde{z}) \frac{2}{\tilde{x}_m^2} \int_0^{\tilde{x}_m} \tilde{x}_\infty \exp\left(-\frac{a}{l_\infty}\phi_\infty(\tilde{x}_\infty)\right) d\tilde{x}_\infty, \tag{33}$$

where $\tilde{x}_m = x_m/a$. Furthermore, we will look into the circumstances where the area-averaged aerosol concentration decays exponentially with increasing number of the layers, separated by the distance $2x_m$, which means that

$$\bar{n}(\tilde{x}_m) = n_\infty(-\tilde{x}_m) \exp\left(-\frac{2x_m}{\bar{l}}\right), \tag{34}$$

wherein $\bar{l}$ is the *effective macroscale filtration length* of the nonuniform filter material. Using equations (34) and (33) jointly with equation (29), one obtains the following expression for $\bar{l}$:

$$\frac{1}{\bar{l}} - \frac{1}{l_\infty} = \frac{1}{2x_m} \ln\left[\frac{2}{\tilde{x}_m^2} \int_0^{\tilde{x}_m} \tilde{x}_\infty \exp\left(-\frac{a}{l_\infty}\phi_\infty(\tilde{x}_\infty)\right) d\tilde{x}_\infty\right]. \tag{35}$$

Since, generally, the volume of the inclusion is proportional to a^3, one has (see Fig. 1)

$$\tilde{x}_m = x_m/a \sim \alpha^{-1/3}. \tag{36}$$

In particular, for spherical inclusions

$$\tilde{x}_m = \sqrt[3]{\frac{2}{3\alpha}}, \tag{36a}$$

which shows that $\tilde{x}_m \gg 1$ when $\alpha \ll 1$. In this limit one can show that the expression in square parentheses in equation (35) is close to unity. Indeed, with increasing $\tilde{x}_\infty$, $\phi_\infty(\tilde{x}_\infty)$ decays to zero as $\tilde{x}_\infty^{-2}$. Therefore, with increasing upper limit of the integral in equation (35) one has $\exp[-a\phi_\infty(\tilde{x}_\infty)/l_\infty] \to 1$ as $\tilde{x}_\infty \to \infty$, and the integrand function approaches $\tilde{x}_\infty$. Bearing in mind the above, we rewrite the integral in equation (35) in the following form:

$$\frac{2}{\tilde{x}_m^2}\int_0^{\tilde{x}_m} \tilde{x}_\infty \exp\left(-\frac{a}{l_\infty}\phi_\infty(\tilde{x}_\infty)\right) d\tilde{x}_\infty = 1 + \frac{2}{\tilde{x}_m^2}\beta(\tilde{x}_m), \tag{37}$$

with $\beta(\tilde{x}_m)$ given by the integral

$$\beta(\tilde{x}_m) = \int_0^{\tilde{x}_m} \tilde{x}_\infty \left[\exp\left(-\frac{a}{l_\infty}\phi_\infty(\tilde{x}_\infty)\right) - 1\right] d\tilde{x}_\infty, \tag{38a}$$

where in view of equation (36)

$$2\frac{\beta(\tilde{x}_m)}{\tilde{x}_m^2} \ll 1, \quad \alpha \ll 1. \tag{38b}$$

Substituting equation (37) into equation (35) and expanding ln in power series using equation (38b), one obtains

$$\frac{1}{\bar{l}} - \frac{1}{l_\infty} = \frac{1.5}{a}\alpha\beta(\tilde{x}_m). \tag{39}$$

The function $\beta(\tilde{x}_m)$ is governed by the asymptotic rate (31b) at which $\phi_\infty(\tilde{x}_\infty)$ vanishes with increasing $\tilde{x}_\infty$. In the particular case of a sufficiently small size of the inclusions and a relatively large l_∞ one can deduce the functional dependence $\beta(\tilde{x}_m)$ by substituting equation (31b) into equation (38a) and expanding the argument of the exponential function in the power series for $a\phi_\infty(\tilde{x}_\infty)/l_\infty \ll 1$, thereby obtaining

$$\beta(\tilde{x}_m) \sim \frac{a}{l_\infty}[C_1' \ln(\tilde{x}_m) + C_2'] \quad \text{as } \tilde{x}_m \to \infty, \tag{40}$$

where C_1', C_2' are independent of $\tilde{x}_\infty$. Introducing equation (40) into equation (39), one finally obtains

$$\frac{\bar{l}}{l_\infty} = \frac{1}{1 + \alpha[C_1 \ln\alpha + C_2 + O(\alpha)]}, \tag{41}$$

with C_1, C_2 being constants expressible via C_1', C_2'.

The above expression constitutes the main result of our analysis. It is derived for inclusions of arbitrary axisymmetric shapes. One can see from equation (41) that the conclusion of whether the effect of inclusions is to increase or decrease the characteristic filtration length depends on the volumetric fraction α and the constants C_1, C_2. These values depend on the precise shape of the inclusion and the filtration properties of the filter material. More detailed considerations of spherical inclusions are given in Section 6.

6. VALIDITY OF DIFFUSIONLESS MESOSCALE AEROSOL TRANSPORT

This section concerns aerosol concentration distribution between subsequent layers of inclusions within the filtering material. This distribution has been assumed uniform

($\tilde{x}_\infty$-independent) far upstream before each layer of inclusions. Therefore, different portions of aerosol particles, which were assumed to move in a diffusionless manner along different trajectories, deposit with different rates. This results in a nonuniform aerosol concentration distribution far downstream from each inclusion. The above model is valid if there exists a mechanism responsible for aerosol redistribution, i.e. remixing leading to a uniform concentration at the upstream of each subsequent layer of inclusion. Such remixing indeed occurs as a result of lateral (in the x-direction) mesoscale aerosol diffusion (dispersion), neglected in the solution in Section 4. This assumption, on the one hand, enables exact solution of the problem. On the other hand, it is justifiable only for relatively short distances (comparable to a).

Summarizing the above, one can formulate the following quantitative criteria for the validity of the model developed above. The effect of the lateral diffusion on particle migration between different streamlines during their motion in the vicinity of an inclusion should be negligible. The characteristic time of their motion in this region is $t_a = a/V_\infty$. During this time the particles migrate at a characteristic distance $(D_x t_a)^{1/2} = (D_x a/V_\infty)^{1/2}$, where D_x is the lateral component of the aerosol mesoscale diffusion coefficient. This distance should be much less than the size a of the inclusion, i.e.

$$(D_x a/V_\infty)^{1/2} \ll a. \tag{42}$$

On the other hand, the characteristic time of motion between two successive particle layers $t_m = x_m/V_\infty$ should be sufficiently large to smear out the nonuniformity of the size a of the downstream aerosol distribution. This leads to the condition

$$(D_x x_m/V_\infty)^{1/2} = O(a). \tag{43}$$

The effective lateral diffusivity (dispersivity) is primarily caused by mechanical, or pure hydrodynamic dispersion and may be correlated by (Adler, 1992)

$$D_x \sim V_\infty d. \tag{44}$$

Using equations (44) and (36) one can rewrite conditions (42) and (43) in the following respective forms:

$$d/a \ll 1. \tag{45}$$

$$d/a \sim O(\alpha)^{1/3}, \tag{46}$$

both of which are satisfied if $\alpha \ll 1$, in accordance with the prior assumption of smallness of the volumetric fraction of inclusions within the porous material.

7. CALCULATION OF THE CHARACTERISTIC FILTRATION LENGTH FOR SPHERICAL INCLUSION

One can obtain the following expressions for the air flow streamlines in the porous material near a spherical inclusion (see Appendix A):

$$r\sin\theta\sqrt{1-\frac{2\xi a^3}{r^3}} = x_\infty, \quad r > a, \tag{47a}$$

$$r\sin\theta = x_\infty/\sqrt{1-2\xi}, \quad r < a \quad (x_\infty < a\sqrt{1-2\xi}), \tag{47b}$$

with x_∞ defined as in Section 2 (see also Fig. 2) and ξ given by equation (A2a).

In the following we denote by x, z, r the corresponding *dimensionless* coordinates (normalized by a). The goal of the following treatment is to calculate $\phi_\infty(x_\infty)$ appearing in equation (32) with the subsequent evaluation of the aerosol filtration length in the form (41). To this goal we calculate f and f_1 appearing in equations 25a, b), separately for the air trajectories which cross the inclusions and those which pass beyond them.

7.1. *Trajectories which do not cross the inclusions* $[x_\infty > (1 - 2\xi)^{1/2}]$

We approximate the trajectory equations (47a) outside an inclusion by replacing x with x_0, related to x_∞ by

$$x_0 = x_\infty \left(1 - \frac{2\xi}{x_0^3}\right)^{-1/2}, \quad x_\infty > (1 - 2\xi)^{1/2}, \tag{48}$$

which represents the coordinate of the trajectory point at $z = 0$. This will not introduce large errors in the calculations, since for small $z \ll a$ $\mathrm{d}x/\mathrm{d}z \sim 0$ along the trajectories; for large $z \gg a$ the expression in the square root of equation (47a) is dominated by z^2 and almost independent of x.

The dimensionless air speed V/V_∞ given by equation (A7a) may be approximated with the help of equation (47a) in the considered region by

$$\frac{V}{V_\infty} \cong 1 + \frac{\xi}{r^3}(\cos 2\theta - 1) \cong 1 - \frac{2\xi}{r^5} \cong 1 - \frac{2\xi x_\infty^2}{(x_0^2 + z^2)^{5/2}}, \tag{49}$$

which yields the following expression for the function $f(z, x_\infty)$ appearing in equation (25a):

$$f(z, x_\infty) = -\frac{2\xi x_\infty^2}{(x_0^2 + z^2)^{5/2}}. \tag{50}$$

Furthermore, using equation (A7a), one obtains the following expression for $f_1(z, x_\infty)$ in equation (25b):

$$f_1(z, x_\infty) = \sqrt{1 + \frac{9\xi^2 x_\infty^2 z^2}{(x_0^2 + z^2)^5}} - 1 \cong \frac{9\xi^2 x_\infty^2 z^2}{2(x_0^2 + z^2)^5}. \tag{51}$$

7.2. *Trajectories which cross the inclusions* $[x_\infty < (1 - 2\xi)^{1/2}]$

The dimensionless air speed V/V_∞ given by equation (A7a) outside an inclusion may be approximated by

$$\frac{V}{V_\infty} \cong 1 + \frac{\xi}{r^3}(2\cos 2\theta - 1). \tag{52}$$

For these trajectories one can determine $f(z, x_\infty)$:

$$f(z, x_\infty) = -\frac{\xi}{(x_0^2 + z^2)^{3/2}} + \frac{4x_\infty \xi}{(x_0^2 + z^2)^{5/2}}, \tag{53}$$

where x_0 is now given by [cf. equation (48)]

$$x_0 = x_\infty (1 - 2\xi)^{-1/2}, \quad x_\infty < (1 - 2\xi)^{1/2}, \tag{54}$$

and designates the x-coordinate of the point of intersection of the trajectory with the inclusion. The expression for the function $f_1(z, x_\infty)$ outside the sphere is identical to equation (51).

Inside the sphere one has

$$f(z, x_\infty) = \frac{\psi(\varepsilon_2)}{\psi(\varepsilon_1)}\zeta - 1 = \gamma = \text{const}, \quad f_1 = 0. \tag{55}$$

Equations (50), (51) and (55) may be used to calculate $\phi_\infty(x_\infty)$ and the macroscopic characteristic filtration length. Details of these calculations are given in Appendix B. As a result, one obtains equation (41) for $\bar{l}$, wherein

$$C_1 = 4\xi/3, \tag{56}$$

$$C_2 = 0.99\xi - 0.143\xi^2 + 1.319\xi^3 + 0.299\xi^4 - 1.455\xi(1 - 2\xi)^{3/2} - (1 - 2\xi)\gamma. \tag{57}$$

8. DISCUSSION

We analyze dependence of the characteristic filtration length (41) with C_1, C_2 given by equations (56) and (57), on the porosity ratio $\varepsilon_2/\varepsilon_1$. Parameter γ in equation (57) depends on the ratio of permeabilities [see equation (55)]. For this ratio we employ the correlation (Davies, 1973, p. 36)

$$\kappa = \frac{a^2}{16(1-\varepsilon)^{3/2}[1+56(1-\varepsilon)^3]}, \tag{58}$$

valid for $\varepsilon < 0.98$. This yields

$$\frac{\kappa_2}{\kappa_1} = \frac{(1-\varepsilon_1)^{3/2}[1+56(1-\varepsilon_1)^3]}{(1-\varepsilon_2)^{3/2}[1+56(1-\varepsilon_2)^3]}. \tag{59}$$

For the ratio $\psi(\varepsilon_2)/\psi(\varepsilon_1)$ the following expression is employed (Brown, 1993, p. 10):

$$\frac{\psi(\varepsilon_2)}{\psi(\varepsilon_1)} = \frac{(1-\varepsilon_1)}{(1-\varepsilon_2)}. \tag{60}$$

To simplify presentation of the data we neglect the term $(1-\varepsilon)^3$ in the square brackets of equation (59), thereby restricting ourselves to sufficiently high porosities $\varepsilon_2, \varepsilon_1$. In this case, C_1, C_2 depend on the ratio of solidities appearing on the right-hand side of equation (60) (see Fig. 3).

For $(1-\varepsilon_2)/(1-\varepsilon_1) = 1$, both C_1, C_2 vanish and the effective filtration lengths is l_∞. One can see, however, that in the limiting case $(1-\varepsilon_2)/(1-\varepsilon_1) \gg 1$ (the inclusions are less porous than the filter matrix) both coefficients tend to approximately the same positive value.

When the solidity ratio $(1-\varepsilon_2)/(1-\varepsilon_1) < 1$ the coefficients plotted in Fig. 3 have different signs. Since in this range $\xi < 0$, and also for all $\alpha \ln \alpha < 0$, one can generally conclude that inclusions, which are more porous than the filter material, lead to a decrease of the aerosol filtration length, i.e. to an enhancement of the aerosol filtration rate.

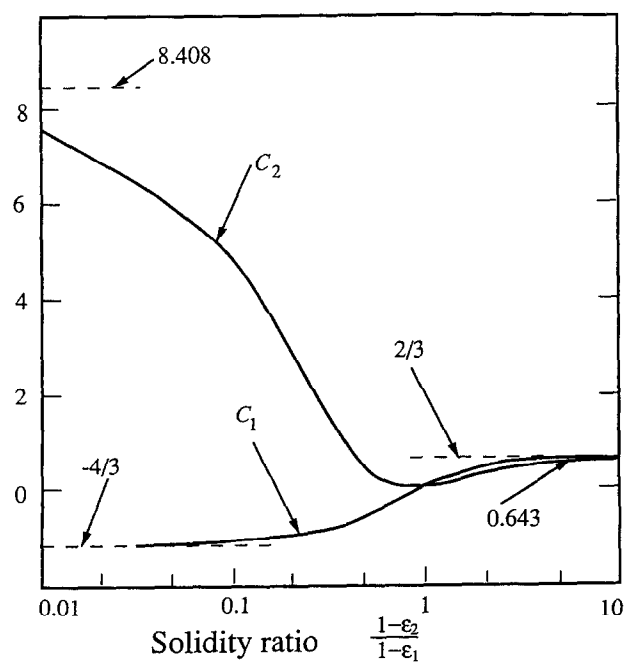

Fig. 3. Coefficients governing the effective aerosol filtration length vs ratio of solidities.

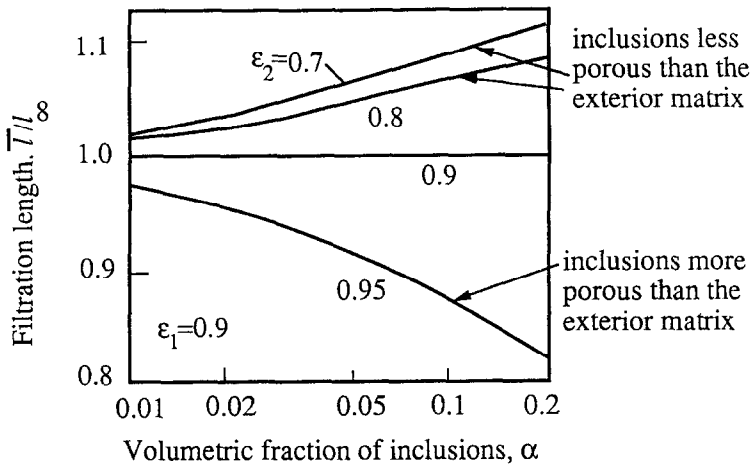

Fig. 4. Aerosol filtration length vs volumetric fraction of inclusions for different porosities.

Figure 4 presents the dependence of the ratio of the characteristic filtration lengths vs α for $\varepsilon_1 = 0.9$ (typical for fibrous filters) and several porosities ε_2 of the inclusions. One can see that in the considered range of small α (less than 0.2) more porous (than the filter material) inclusions improve the filtration capacity. The less porous inclusions lead to a deterioration of the aerosol collection rate. In particular, our model predicts that a slight difference in porosities, $\varepsilon_2 - \varepsilon_1 = 0.05$, leads to 20% decrease of the filtration length.

Conclusion as to whether the effect of material inhomogeneities is to increase or decrease the effective filtration length in the whole range of solidity ratio, depends both upon the value of $(1 - \varepsilon_2)/(1 - \varepsilon_1)$ and the volumetric fraction α. In particular, given the fact that in the range $(1 - \varepsilon_2)/(1 - \varepsilon_1) > 1$ the plotted coefficients are both approximately equal to 2/3, one can see that the effective filtration length increases when $\ln\alpha < -1$, i.e. $\alpha < 0.368$. Therefore, less porous (than the filter matrix) inclusions tend to decrease aerosol filtration efficiency for small α with the reverse trend prevailing for larger volumetric fractions. In the following section we provide an experimental verification of this theoretical prediction.

9. FILTRATION LENGTH OF A NONHOMOGENEOUS POLYDISPERSE GRANULAR BED

Verification of the analytical model may be done on the basis of more accurate (numerical) integration of equation (21) for any given spatial distribution of inhomogeneities. This will be the subject of future investigations. An experimental check of the model prediction should be done using a filtering material, for which the mesoscale distribution of porosities may be measured. One such material is polydisperse packed beds. In the case where the bed is composed of granules of two different sizes, one can view small granules as a porous matrix and each large granule as an (impermeable) inclusion.

The effective filtration length of a composite material of the above type can be calculated by using the permeability of inclusion $\kappa_2 = 0$ in equation (A2), which yields $\xi = 1/2$. Further simplifying equations (56) and (57) one can reduce equation (41) to the form

$$\frac{\bar{l}_\infty}{l_\infty} = \frac{1}{1 + \alpha[0.667 \ln\alpha + 0.643]}, \tag{61}$$

where α is the volumetric fraction of large granules. The calculated ratio $\bar{l}/l_\infty$ is shown in Fig. 5, and exhibits a nonmonotic α-dependence, i.e. it increases with α for small $\alpha < 0.364$ with the reverse trend prevailing for larger volumetric fractions.

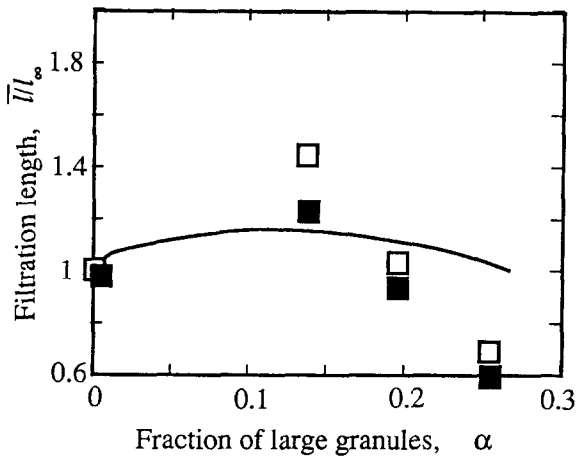

Fig. 5. Comparison of the calculated effective aerosol filtration length (solid line) with the experimental data collected for latex aerosol particles by granular beds. The bed is composed of glass spheres of two sizes: 1.4 and 15 mm. Hollow symbols: aerosol $d_p = 0.1$ μm, air velocity $V = 0.25\,\mathrm{cm\,s^{-1}}$; filled symbols; $d_p = 0.24$ μm, $V = 1.05\,\mathrm{cm\,s^{-1}}$.

Here we provide an experimental test of the above predictions for a bidisperse filter medium composed of glass spherical beads of two different sizes. Explicitly, the porous filter matrix was formed by a packed bed of 1.4 mm spheres, wherein larger spheres of diameter 15 mm served as inclusions. The granular beds were prepared for different volumetric fractions α of larger spheres, ranging from 0 to 26%. The bed thickness was 10 cm and the diameter was 5 cm. The filtration efficiencies of 0.1 and 0.24 μm latex aerosol particles produced by the Royco aerosol generator, and passed through the TSI Electrostatic Classifier were measured with the filter face velocities of 0.25 and $1.05\,\mathrm{cm\,s^{-1}}$. Measurements were performed in the steady regime using the TSI Condensation Particle Counter.

The results of the measurements are shown in Fig. 5. One can see that the theoretical nonmonotonic α-dependence is qualitatively confirmed by the experimental data. Physically, the increase of $\bar{l}/l_\infty$, observed for small α (less than 14%), stems from the air acceleration in the vicinity of larger spheres, which results in a lower diffusional collection rate [see equation (23a)]. For larger α the filtration efficiency increases ($\bar{l}/l_\infty$ decreases) due to increasing length of aerosol mesoscale trajectory within the filter matrix. For larger α this factor becomes dominant and effectively controls the aerosol deposition in nonhomogeneous granular filters.

The above qualitative comparison cannot be viewed as a quantitative assessment of the merits of the proposed model. Strictly speaking, the limit $\varepsilon_2 \to 0$ (impermeable inclusions) is not described by the model here proposed, since in the immediate vicinity of a large granule the Darcy law 6(a, b) is no longer valid. Calculation of the air velocity distribution and aerosol collection rate in this region requires incorporation of a more general Brinkman law (Neal and Nader, 1974). Additional sources of discrepancies between the model predictions and the experimental data in Fig. 5 may be filtration mechanisms (e.g. gravitation, interception), which are disregarded in the course of derivation of equation (61). Moreover, hydrodynamic interactions between the neighboring inclusions (which are also neglected) affect mesoscale air streamlines. These interactions play a major role for large α, for which equation (41) is no longer valid.

10. CONCLUDING REMARKS

In this paper a general model is developed for calculation of the aerosol collection rate by a porous filtering material for a given spatial distribution of porosity. Calculations performed for a special material structure e.g. for a small volumetric fraction α of inclusions,

embedded within a homogeneous matrix, exhibited the effect of the filter nonuniformity, and porosity of inclusions. Several simplifying assumptions pertaining to the geometric model employed here enabled derivation of a simple analytical expression (41) for the effective filtration length. The α-dependence of the effective filtration length as predicted by this formula was qualitatively confirmed by aerosol collection experiments performed for bidisperse granular bed filters. However, more experimental tests are required to evaluate the predictive capacity of the model for nonhomogeneous granular and fibrous filtering materials.

Approximate analytical derivations of equation (41) can be generalized by relaxing the assumption of the smallness of the volumetric fraction α of the inclusions. This can be done by considering the cell-like Kuwabara-type geometric models to describe the mesoscale velocity distribution. Additionally, information about the collector (fiber) diameter distributions and their orientations, both inside and outside the inclusions, as well as different particle capture mechanisms, can be incorporated in the aerosol mesoscale collection laws (23a, b).

One advantage of the present model is that it enables incorporation of all the above information at the mesoscale level, i.e. for a representative volumetric element surrounding one inclusion, with subsequent integration over the whole filter material volume. In this sense the treatment proposed here parallels the classical filtration theory (Davies, 1973) developed for homogeneous filters.

Instead of analytical solution, an alternative, more straightforward approach is integration of equations (7) and (8) for a given porosity distribution. The air velocity field obtained from this solution and the data on the aerosol mesoscale transport and deposition coefficients may be used to solve equation (19). This would involve a significant computational effort, comparable to that required in the spatial elements' model of Schweers and Löffler (1993).

Acknowledgements—This research was supported in part by the Israel Ministry of Science and Technology. The author is thankful to Prof. H. Fissan and Dr W. Mölter for fruitful discussions, stimulating the performance of this study and to Dr S. Lekhtmakher for measuring the filtration efficiencies of glass bed filters. Comments of Dr E. Schmidt, Dr T. Lücke and Dr G. Kasper to a previous version of this manuscript are gratefully acknowledged.

REFERENCES

Adler, P. M. (1992) *Porous Media. Geometry and Transports.* Butterworth-Heinemann, Boston.

Bear, J. (1972) *Dynamics of Fluids in Porous Media.* American Elsevier, New York.

Bird, R. B., Stewart, W. E. and Lightfoot, E. N. (1960) *Transport Phenomena.* Wiley, New York.

Brown, R. C. (1993) *Air Filtration. An Integrated Approach to the Theory and Applications of Fibrous Filters.* Pergamon Press, Oxford.

Davies, C. N. (1973) *Air Filtration,* Academic Press, London.

Dorman, R. G. (1974) *Dust Control and Air Cleaning.* Pergamon Press, Oxford.

Ives, K. J. (1986) Deep bed filters. In *Solid–Liquid Separation Equipment Scale-Up,* 2nd Edition (Edited by Purchas, D. B. and Wakeman, R. J.), pp. 333–363. Upland Press, London.

Lajos, T. (1985) *Staub. Reinh. Luft.* (Suppl. 1) **45,** 19–23.

Leers, R. (1957) Die Abscheidung von Schwebstoffen in Faserfiltern. *Staub. Reinh. Luft.* **17,** 402–417.

Levich, V. G. (1962) *Physicochemical Hydrodynamics.* Prentice-Hall, Englewood Cliffs, NJ.

Lücke, T., Adam, R. and Tittel, R. (1993) Macroscopic modeling of filtration performance of inhomogeneous filter materials for high efficient air filters. *J. Aerosol Sci.* (Suppl. 1) **24,** S565–S566.

Maxwell, J. C. (1881) *A Treatise on Electricity and Magnetism,* Vol. 1. Clarendon Press, Cambridge.

Morse, P. M. and Feshbach, H. (1953) *Methods of Theoretical Physics,* Vol. II. McGraw-Hill, New York.

Neal, H. N. and Nader, W. K. (1974) Prediction of transport process within porous media: slow motion of fluids relative to beds of spherical particles. *A.I.Ch.E. J.* **20,** 530.

Pich, J. (1966) Theory of aerosol filtration by fibrous and membrane filters. In *Aerosol Science* (Edited by Davies, C. N.). Academic Press, London.

Schweers, E. and Löffler, F. (1993) Behavior of industrial fibrous filters—experimental investigation and realistic modelling through the consideration of inhomogeneities. *J. Aerosol Sci.* (Suppl. 1) **24,** S563–S564.

Shapiro, M. and Brenner, H. (1990) Dispersion–reaction model of aerosol filtration by porous filters. *J. Aerosol. Sci.* **21,** 97–125.

Shapiro, M., Kettner, I. J. and Brenner, H. (1991) Transport mechanics and collection of submicrometer particles in fibrous filters. *J. Aerosol Sci.* **22,** 707–722.

Tardos, G. I., Abuaf, N. and Gutfinger, C. (1978) Dust deposition in granular bed filters. Theories and experiments. *JAPCA* **28,** 354.

APPENDIX A: THE MESOSCALE AIR VELOCITY AND PRESSURE DISTRIBUTION AROUND A SPHERICAL INCLUSION

For spherical inclusions of radius a equations (7) and (8) reduce to

$$\nabla^2 P \equiv \frac{1}{r^2}\frac{\partial}{\partial r}\left(r^2\frac{\partial P}{\partial r}\right)+\frac{1}{r^2\sin\theta}\frac{\partial}{\partial r}\left(\sin\theta\frac{\partial P}{\partial r}\right)=0, \tag{A1a}$$

to be solved in the two domains $0<r<a$ and $a<r<\infty$ subject to the boundary conditions

$$P(a+0,\theta)=P(a-0,\theta), \tag{A1b}$$

$$\kappa_1\frac{\partial P}{\partial r}(a+0,\theta)=\kappa_2\frac{\partial P}{\partial r}(a-0,\theta), \tag{A1c}$$

and condition (9) in the infinity.

Problem (A1), (9) is identical to the problem of distribution of the electrostatic potential within a homogeneous material with a spherical inclusion of a different dielectric constant. The solution of this problem is given by Maxwell (1881) and may be expressed in the form [cf. equations (11) and (13)]

$$P=\left(\frac{dP}{dz}\right)_\infty \zeta r\cos\theta+\text{const}, \quad 0<r<a, \tag{A2a}$$

$$P=\left(\frac{dP}{dz}\right)_\infty \left(\frac{a^3}{r^3}\xi+1\right)r\cos\theta+\text{const}, \quad a<r<\infty, \tag{A2b}$$

where the constants ξ, ζ are

$$\xi=\frac{1-\kappa_2/\kappa_1}{2+\kappa_2/\kappa_1}, \quad \zeta=\frac{3}{2+\kappa_2/\kappa_1}. \tag{A2c, d}$$

Solution (A2a–d) may be used to calculate the effective permeability $\bar{\kappa}$ of the nonhomogeneous porous material:

$$\bar{\kappa}=\kappa_1\frac{1-2\alpha\xi}{1+\alpha\xi}, \tag{A3}$$

valid for small values of the volumetric fraction α. Explicitly, $\bar{\kappa}$ relates the pressure drop across the filter with the macroscale, area-averaged air velocity $\bar{V}$:

$$\bar{V}=-\frac{\bar{\kappa}\Delta\bar{P}}{\mu L}. \tag{A4}$$

The components of the velocity field are obtained by the introduction of equations (A2a, b) into equation (6b):

$$V_r=\begin{cases}V_\infty(1-2\xi a^3/r^3)\cos\theta, & a<r<\infty,\\ V_\infty\zeta\cos\theta, & 0<r<a,\end{cases} \tag{A5a}$$

$$V_\theta=\begin{cases}-V_\infty(1+\xi a^3/r^3)\sin\theta, & a<r<\infty,\\ -V_\infty\zeta\sin\theta, & 0<r<a.\end{cases} \tag{A5b}$$

The air flow streamlines through the porous material are obtained by solving the differential equation (15) together with formulas (A5a, b) [cf. equation (16)]:

$$r\sin\theta\sqrt{1-\frac{2\xi a^3}{r^3}}=x_\infty, \quad r>a, \tag{A6a}$$

$$r\sin\theta=x_\infty/\sqrt{1-2\xi}, \quad r<a, \quad (x_\infty<a\sqrt{1-2\xi}), \tag{A6b}$$

with the meaning of x_∞ as in Section 2.

The air speed V/V_∞ outside and inside the inclusion is

$$\frac{V}{V_\infty}=\left[1+\frac{\xi}{(r/a)^3}(3\cos 2\theta-1)+\frac{\xi^2}{2(r/a)^6}(5-3\cos 2\theta)\right]^{1/2}, \quad r>a, \tag{A7a}$$

$$\frac{V}{V_\infty}=\zeta, \quad 0<r<a. \tag{A7b}$$

APPENDIX B: CALCULATION OF $\phi_\infty(x_\infty)$

For calculations of $\phi_\infty(x_\infty)$ we neglect $f(z, x_\infty)$ (as compared to unity) in the denominator of equation (31a). The integration with respect to z may be performed independently for the trajectories crossing the inclusion and

passing exterior to it. Therefore, one has in accordance with equations (50) and (51) for $x_\infty > (1-2\xi)^{1/2}$

$$\phi_\infty(x_\infty) \cong -\int_{-\infty}^{\infty} [f_1(z, x_\infty) - f(z, x_\infty)]\,\mathrm{d}z = \frac{2\xi x_\infty^2}{x_0^4}\int_{-\infty}^{\infty}\frac{\mathrm{d}w}{(1+w^2)^{5/2}} - \frac{9\xi^2 x_\infty^2}{2x_0^7}\int_{-\infty}^{\infty}\frac{w^2\,\mathrm{d}w}{(1+w^2)^5}. \tag{B1}$$

Calculating the integrals

$$\int_{-\infty}^{\infty}\frac{\mathrm{d}w}{(1+w^2)^{5/2}} = \frac{4}{3}, \quad \int_{-\infty}^{\infty}\frac{w^2\,\mathrm{d}w}{(1+w^2)^5} = \frac{5\pi}{128},$$

one can rewrite equation (B1) in the form

$$\phi_\infty(x_\infty) = \frac{8\xi x_\infty^2}{3x_0^4} - \frac{45\pi\xi^2 x_\infty^2}{256x_0^7}, \quad x_\infty > (1-2\xi)^{1/2}. \tag{B2}$$

One can see that this large x_∞ dependence of $\phi_\infty(x_\infty)$ accords with the general prediction (31b).

The expression for $\phi_\infty(x_\infty)$ for $x_\infty < (1-2\xi)^{1/2}$ is obtained by the introduction of equations (50), (51), (53) and (55) into equation (31a) and also neglecting f in the denominator:

$$\begin{aligned}\phi(x_\infty) &= 2\int_{z_0}^{\infty}\left[-\frac{\xi}{(x_0^2+z^2)^{3/2}} + \frac{4x_\infty\xi}{(x_0^2+z^2)^{5/2}} + \frac{9\xi^2 x_\infty^2 z^2}{2(x_0^2+z^2)^5}\right]\mathrm{d}z + 2\int_0^{z_0}\gamma\,\mathrm{d}z \\ &= -\frac{2\xi}{x_0^2}I_1 + \frac{8x_\infty\xi}{x_0^4}I_2 + \frac{9\xi^2 x_\infty^2}{x_0^9}I_3 + 2z_0\gamma.\end{aligned} \tag{B3}$$

In the above

$$z_0 = \sqrt{1 - \frac{x_\infty^2}{1-2\xi}} \tag{B4}$$

is the coordinate of intersection of the trajectory with the inclusion and I_1, I_2, I_3 are given by

$$\begin{aligned}I_1 &= \int_{\psi_0}^{\pi/2}\cos\psi\,\mathrm{d}\psi = 1 - \sin\psi_0, \quad I_2 = \int_{\psi_0}^{\pi/2}\cos^3\psi\,\mathrm{d}\psi = \tfrac{2}{3} - (\sin\psi_0 - \tfrac{1}{3}\sin^3\psi_0), \\ I_3 &= \int_{\psi_0}^{\pi/2}(\cos^6\psi - \cos^8\psi)\,\mathrm{d}\psi \\ &= \frac{5\pi}{128} - \tfrac{1}{32}(\tfrac{5}{4}\psi_0 + \tfrac{1}{2}\sin 2\psi_0 - \tfrac{1}{4}\sin 4\psi_0 - \tfrac{1}{6}\sin 6\psi_0 - \tfrac{1}{32}\sin 8\psi_0),\end{aligned} \tag{B5}$$

and (see Fig. 2)

$$\psi_0 = \arcsin z_0 = \arcsin\sqrt{1 - \frac{x_\infty^2}{1-2\xi}}. \tag{B6}$$

Expression (B3) for $\phi_\infty(x_\infty)$ is too complicated for performing analytical integration with respect to x_∞. Hence, for the latter purpose it has been approximated by

$$\begin{aligned}\phi_\infty(x_\infty) \cong\ & 2\gamma\sqrt{1-x_0^2} + \tfrac{9}{2}\xi^2 x_\infty^2(0.2857 - 0.163x_0^2) + 4\xi x_\infty(\tfrac{1}{2} + \tfrac{5}{6}x_0^8) \\ & - \frac{\xi}{\sqrt{1-x_0^2}+1}, \quad x_\infty < (1-2\xi)^{-1/2},\end{aligned} \tag{B7}$$

with x_0 given by equation (54).

Expressions (B2) and (B7) are to be substituted into equation (38a) for performing subsequent integration with respect to x_∞. Under the condition $a\phi_\infty(\tilde{x}_m)/l_\infty \ll 1$ (implying that the size that the size of inclusions is small compared with the filtration length of the filter material at infinity) which greatly simplifies the integration procedure, one obtains equation (41), wherein C_1, C_2 are given by equations (56) and (57), respectively.